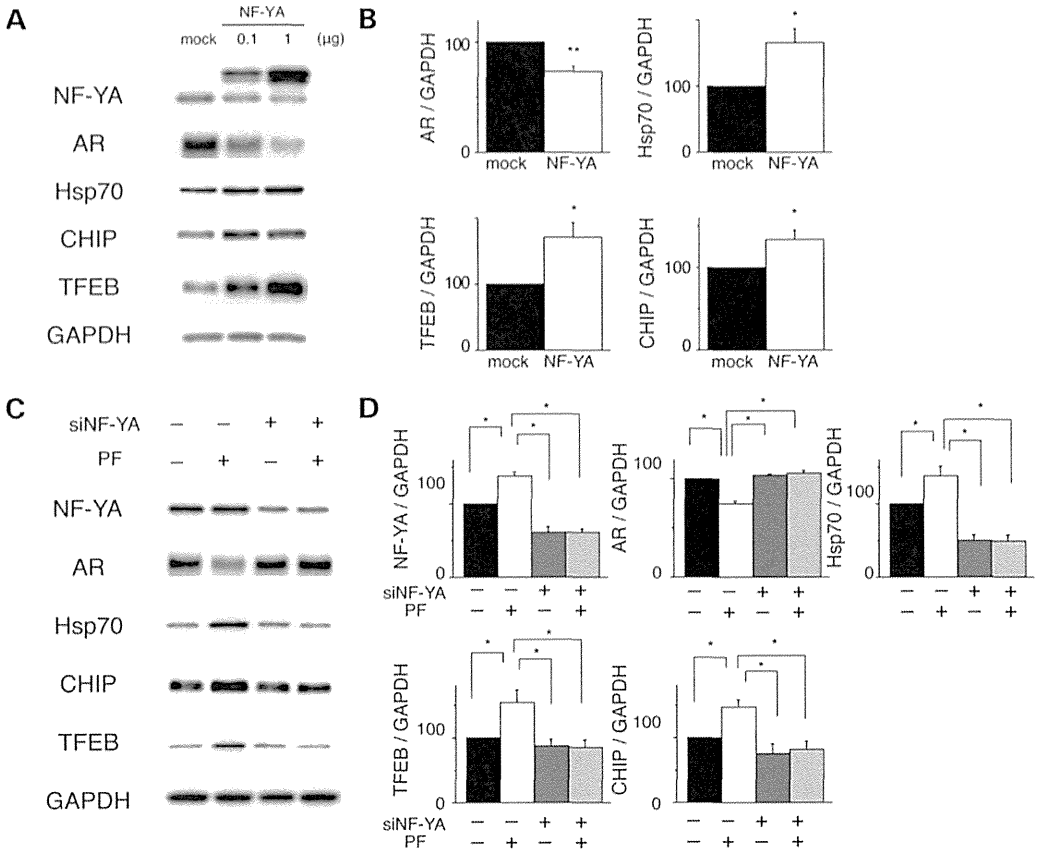

Figure 2. Effects of NF-YA overexpression in cultured cell models of SBMA. (**A** and **B**) Western blots and densitometric analyses of NSC34 cells stably expressing mutant AR. Cells were transfected with NF-YA with a V5 tag or the mock vector (*$P < 0.05$; **$P < 0.01$, $n = 5$, unpaired *t*-test). (**C** and **D**) Western blots and densitometric analyses of NSC34 cells stably expressing mutant AR that were transfected with control or NF-YA siRNA and treated with or without PF (*$P < 0.05$, $n = 5$, one-way ANOVA with Tukey–Kramer *post hoc* test). Error bars (B and D), SEM.

We hypothesized that if PF contributes to the activation of autophagy, then the expression of the mutant polyQ protein would be reduced by TFEB-activated autophagy in addition to the UPS degradation. To test this hypothesis, the nuclear translocation of TFEB was investigated using western blot analysis, which showed that PF increased the amount of TFEB in the nucleus at a dose of 10 μM in NSC34 cells (Fig. 3A and B). Next, we investigated whether TFEB promotes the degradation of mutant AR. NSC34 cells stably expressing AR-24Q or AR-97Q were transfected with the indicated amount of TFEB or mock transfected (Fig. 3C). After 48 h, the expression levels of both AR-24Q and AR-97Q similarly decreased following the overexpression of TFEB (Fig. 3C and D). The expression of the autophagic marker LC3-II was significantly elevated in the cells expressing AR-24Q or AR-97Q (Fig. 3C and D), suggesting that the high expression of TFEB induced autophagosome formation and enhanced the degradation of the AR proteins. However, there were no significant differences in the reduction rate between the wild-type and mutant AR (Fig. 3C and D), which indicates that the activation of UPS is the basis for preferential degradation of the polyQ-expanded mutant AR following PF treatment.

PF ameliorates the phenotype of male AR-97Q mice

To verify that PF-mediated activation of the proteolytic machinery mitigates polyQ toxicity, we administered PF intraperitoneally every day at doses of 6.7 mg/kg (PF1) or 13.4 mg/kg (PF2) to males of the transgenic mouse model carrying the full-length human AR with either 24Q or 97Q (21). To demonstrate that PF slows the onset and progression of the disease, PF treatments were initiated when the mice reached 5 weeks of age and continued until they were 32 weeks old. The AR-97Q mice displayed progressive muscular atrophy and weakness that was accompanied by diffuse nuclear accumulation and NIs of mutant AR in neuronal and non-neuronal tissues (21). We examined various neurological and behavioral parameters. In the AR-97Q mice treated with 13.4 mg/kg PF (PF2), the phenotype and disease progression were markedly ameliorated, and the progression in mice treated with 6.75 mg/kg PF (PF1) was moderately ameliorated (Fig. 4A–F). The untreated AR-97Q mice (PF0) exhibited motor impairments (assessed by the rotarod task), as early as 9 weeks after birth, whereas the PF2 group showed initial impairments at 13 weeks after birth and had less deterioration than the PF0 mice (Fig. 4A). The PF1 mice exhibited intermediate levels of impairment in their

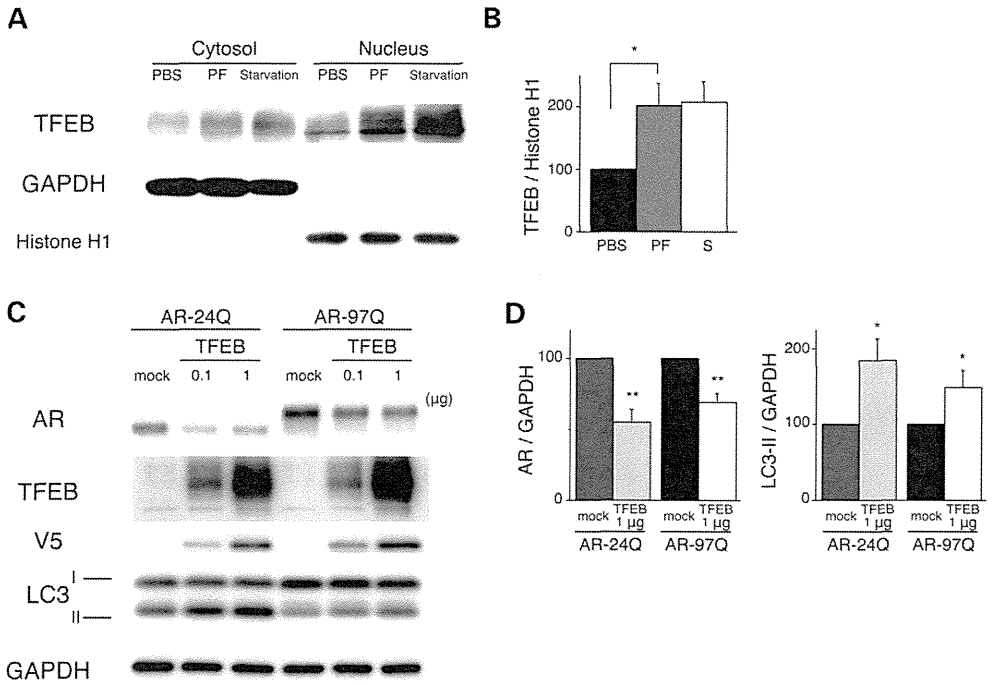

Figure 3. Effects of PF on expression levels of AR via TFEB activation. (**A** and **B**) PF facilitates the nuclear translocation of TFEB. Western blots and densitometric analyses from NSC34 cells treated with 10 μM PF or starvation. Cell lysates were subjected to nuclear or cytosolic fractionation and probed with a TFEB antibody. GAPDH and H1 were used as cytosolic and nuclear markers, respectively (*$P < 0.01$, $n = 5$, one-way ANOVA with Tukey–Kramer *post hoc* test). (**C** and **D**) Effects of TFEB overexpression on the expression levels of wild-type (24Q) and mutant (97Q) ARs in NCS34 cells. Western blots and densitometric analyses from NSC34 cells stably expressing AR-24Q or AR-97Q. Cells were transfected with the mock or TFEB-V5 vector (*$P < 0.01$, $n = 5$, unpaired *t*-test). Error bars (B and D), SEM.

rotarod performance (Fig. 4A). The locomotor cage activity of the PF0 mice was also markedly decreased at 15 weeks compared with the PF1 and PF2 groups, which exhibited decreases in activity at 24 and 26 weeks of age, respectively (Fig. 4B). No mouse lines were distinguishable in terms of body weight at birth; however, the PF0 mice lost weight significantly earlier (by 16 weeks) and to a greater extent than the PF1 and PF2 mice (Fig. 4C). PF treatment also significantly prolonged the lifespan of the PF1 and PF2 mice compared with the PF0 mice (Fig. 4D). Additionally, the PF0 mice exhibited motor weakness, as demonstrated by the dragging of their legs and shortened steps, whereas the PF2 mice had nearly normal ambulation (Fig. 4E and F). AR-24Q mice treated with PF did not have altered phenotypes (Supplementary Material, Fig. S4A–D). To evaluate the possible toxic effects of PF, we examined blood samples from 16-week-old AR-97Q mice treated with 13.4 mg/kg PF for 11 weeks. Measurements of aspartate aminotransferase, alanine aminotransferase, blood urea nitrogen and serum creatinine demonstrated that PF resulted in neither infertility nor liver or renal dysfunction in the AR-97Q male mice (Supplementary Material, Fig. S5A–D). The serum testosterone levels were unchanged in the PF2 mice (1.029 ± 0.369 ng/ml, $n = 15$) versus the PF0 mice (0.857 ± 0.406 ng/ml, $n = 15$).

PF reduces diffuse nuclear staining of mutant AR and degrades mutant AR protein in the mouse model of SBMA

Having demonstrated that PF promotes mutant AR degradation *in vitro*, we examined the levels of AR in the AR-24Q and AR-97Q mice. We performed immunohistochemical staining for mutant AR using the 1C2 antibody in the spinal cord and skeletal muscle of 16-week-old AR-97Q mice. In the PF0 mice, intense staining was frequently observed in the nuclei, whereas staining was infrequent in the PF1 mice and much less frequent in the PF2 mice (Fig. 5A). There were significantly more 1C2-positive cells in the spinal cord and muscle tissue of the PF0 mice than in the PF1 and PF2 mice (Fig. 5B). The 1C2-positive cell populations were not significantly different between the PF1 and PF2 mice (Fig. 5B). There were no NIs in the spinal cord and skeletal muscle of the AR-24Q mice (Supplementary Material, Fig. S4E and F).

Treatment with PF markedly diminished both the high-molecular-weight complex and monomeric mutant AR in the spinal cord and muscle of AR-97Q mice ($P < 0.01$). PF significantly diminished the wild-type monomeric AR in AR-24Q mice (Fig. 5C and D). In the PF2 mice, monomeric AR decreased by 68.5 and 34.5% in the spinal cord and by 50.3 and 37.2% in the skeletal muscle for the AR-97Q and AR-24Q mice, respectively (Fig. 5C and D). Thus, the rate of reduction of the monomeric mutant AR was significantly higher than for wild-type AR in both the spinal cord ($P < 0.01$) and skeletal muscle ($P < 0.01$). Reverse transcription (RT)–polymerase chain reaction (PCR) of both the AR-24Q and AR-97Q mice showed that the levels of AR mRNA were similar in the spinal cord and muscle of the treated (PF2) and untreated (PF0) mice (Fig. 5E and F); thus, the decreased

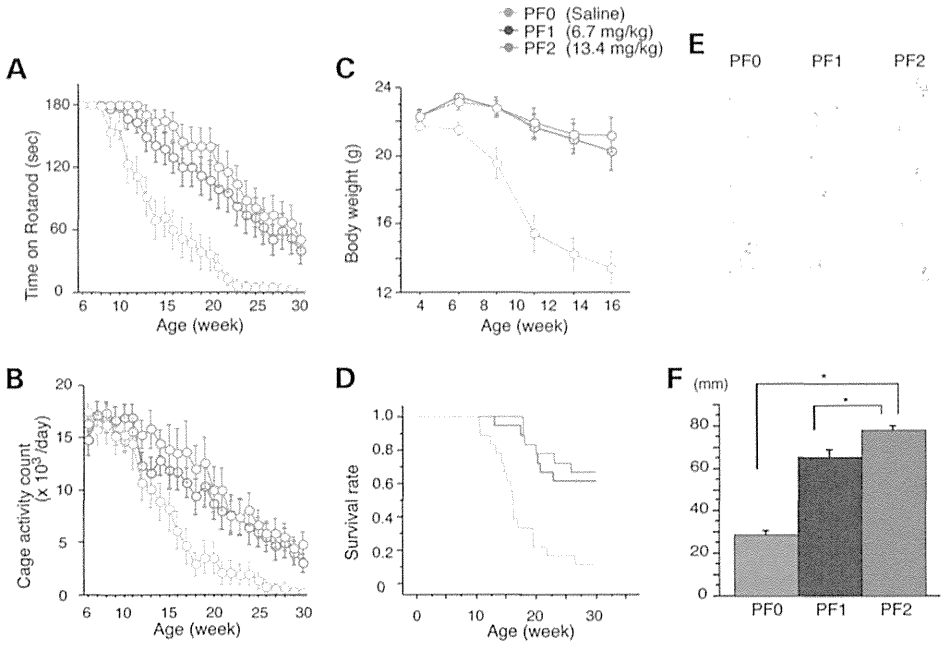

Figure 4. Effects of PF on behavioral phenotypes in AR-97Q mice. Untreated AR-97Q mice (PF0) or mice administered 6.7 mg/kg (PF1) or 13.4 mg/kg (PF2) PF intraperitoneally every day from ages 5 to 30 weeks were tested for rotarod performance (**A**), cage activity (**B**) and body weight (**C**). PF1 and PF2 mice remained on the rotarod longer and exhibited greater cage activity than PF0 mice. PF0 mice lost weight earlier than PF1 and PF2 mice. All parameters were significantly different in PF2 mice compared with PF0 mice: $P < 0.01$ at 25 weeks (rotarod and cage activity) and $P < 0.01$ at 10 weeks (body weight) ($n = 18$, two-way ANOVA with Tukey–Kramer *post hoc* test). (**D**) A Kaplan–Meier plot shows the prolonged survival of PF1 and PF2 mice compared with PF0 mice ($P = 0.0002$ and 0.0001, respectively; $n = 18$, log-rank test). (**E**) Footprints of representative 16-week-old AR-97Q mice treated with or without PF. Front paws are indicated in red, and hind paws are in blue. PF0 mice exhibited motor weakness, demonstrated by the dragging of the legs. PF1 mice walked with somewhat longer steps, and PF2 mice walked almost normally. (**F**) The length of the steps was measured in 16-week-old AR-97Q mice. Each column shows the average length of the steps of the hind paw. PF1 and PF2 mice walked with significantly longer steps than PF0 mice ($^*P < 0.01$, $n = 6$, one-way ANOVA with Tukey–Kramer *post hoc* test). These data suggest that PF ameliorates the phenotypic expression of SBMA in AR-97Q mice in a dose-dependent manner. Error bars (F), SEM.

protein level was due to degradation and not to lower mRNA levels. These observations indicate that PF markedly degrades not only the high-molecular-weight mutant AR complex but also the monomeric mutant AR protein compared with the wild-type AR, which reflects the preferential degradation of the mutant AR through the UPS.

Anti-glial fibrillary acidic protein (GFAP) staining showed an apparent reduction in reactive astrogliosis in the PF2 mice in the spinal anterior horn (Fig. 5G). Muscle histology also demonstrated a marked amelioration of muscle atrophy in the PF2 mice (Fig. 5H).

Effect of PF on the regulation of proteolytic machinery *in vivo*

Both low and high doses of PF treatment of the SBMA transgenic mice were accompanied by marked increases in NF-YA mRNA levels and protein synthesis in the spinal cord and muscle tissue (Fig. 6A–F). These results were well correlated with those of anti-NF-YA immunohistochemical-stained tissue sections (Supplementary Material, Fig. S6A and B). In contrast, PF treatment in the cell and mouse models of SBMA had no effect on the expression levels of hyper-phosphorylated heat shock factor-1 (10,22), p53 (23) or transcription factors regulating Hsp expression, namely, TBP and SP1 (Supplementary Material, Fig. S2A). AR-97Q transgene expression decreased the expression level of NF-YA in both the spinal cord and muscle (Fig. 6C and D). This effect might be due to a decrease in mRNA levels (Fig. 6A and B) and sequestration of endogenous NF-YA in the inclusions in the spinal anterior horn cells and muscle tissue of AR-97Q mice; this finding was also observed in the spinal anterior horn cells of SBMA patients (Supplementary Material, Fig. S6A and B). To ensure that PF activated the proteolytic machinery *in vivo*, the expression levels of the molecular chaperones, CHIP and TFEB, were determined using western blotting. In the AR-24Q and AR-97Q mice, the levels of Hsp70, Hsp40, CHIP and TFEB were significantly increased (Fig. 6C–F), and PF facilitated the nuclear translocation of TFEB in the spinal cord and muscle of the AR-24Q and AR-97Q mice (Supplementary Material, Fig. S7). Furthermore, western blotting showed that PF treatment resulted in increased expression levels of lysosomal proteases and the autophagic marker LC3-II in the spinal cord and muscle of the AR-24Q and AR-97Q mice (Fig. 7A–D). The expression level of protease mRNA also increased in the AR-24Q and AR-97Q mice treated with 13.4 mg/kg PF as well as in the cell culture model treated with 10 μM PF (Supplementary Material, Fig. S8A–C). These observations suggest that an increase in the levels of the molecular chaperones CHIP and TFEB promotes the downregulation of ARs via the UPS and autophagic

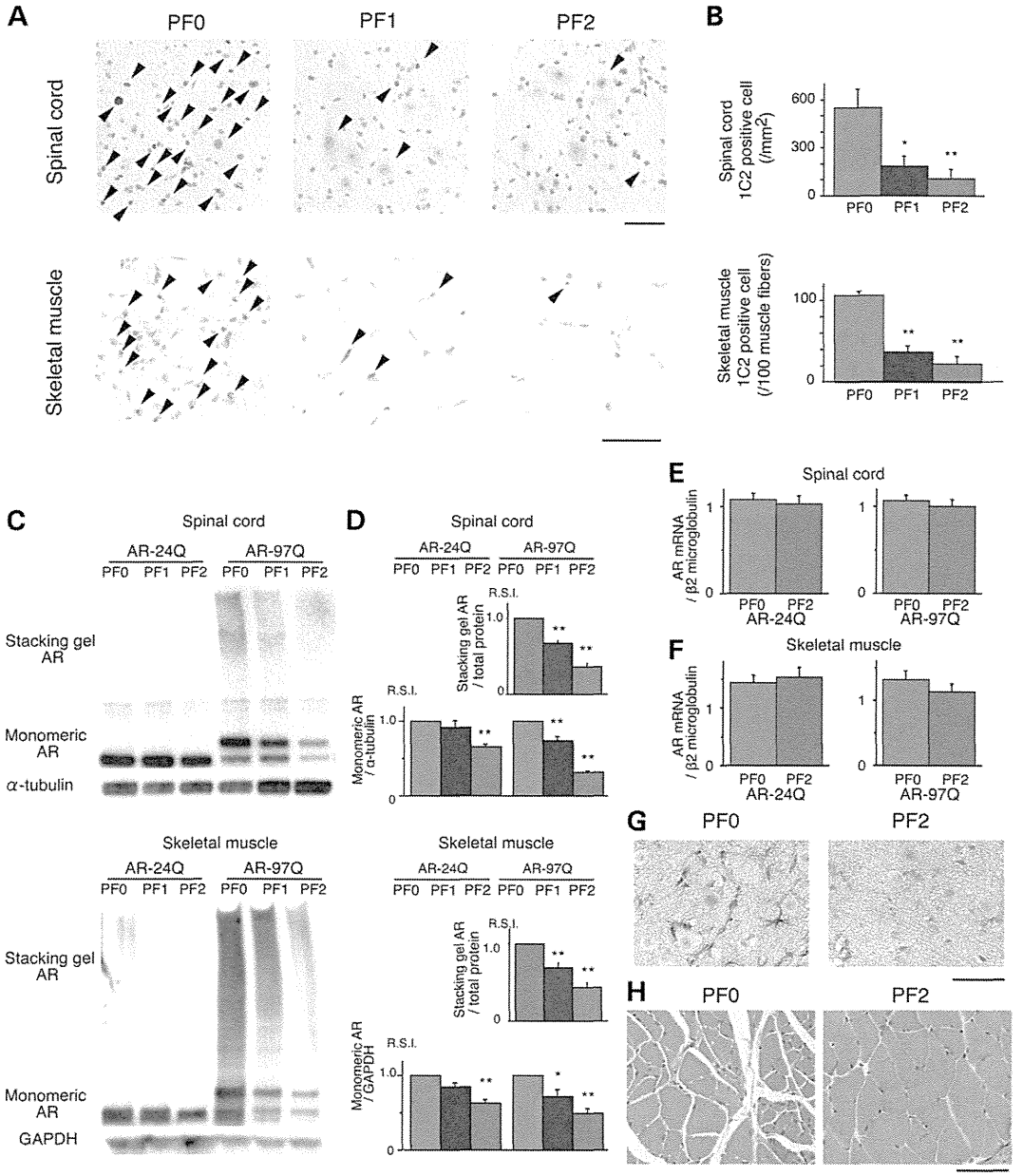

Figure 5. Effects of PF on the nuclear accumulation of abnormal AR in 16-week-old AR-24Q and AR-97Q mice. (**A**) Immunohistochemical staining for mutant AR using the 1C2 antibody showed a marked reduction in diffuse nuclear staining and NIs (arrow head) in the spinal cord and skeletal muscle of the treated mice compared with the PF0 mice. (**B**) Quantification of the number of 1C2-positive cells in the spinal cord and skeletal muscle of AR-97Q mice treated with or without PF (*$P < 0.05$; **$P < 0.01$, $n = 6$, one-way ANOVA with Tukey–Kramer *post hoc* test). (**C** and **D**) Western blot analysis of total tissue homogenates from the spinal cord and muscle of AR-24Q and AR-97Q mice probed with anti-AR (*$P < 0.05$; **$P < 0.01$, $n = 5$, one-way ANOVA with Tukey–Kramer *post hoc* test). (**E** and **F**) Real-time RT–PCR of wild-type and mutant AR mRNA in the spinal cord (E) and skeletal muscle (F). Quantities are presented as the ratio to β2 microglobulin mRNA ($n = 5$, unpaired *t*-test). (**G**) Immunohistochemical staining with anti-GFAP antibody in the spinal anterior horn of AR-97Q mice. (**H**) Hematoxylin and eosin staining of the muscles of AR-97Q mice. Error bars (B, D, E and F), SEM. Scale bars: 50 μm.

degradation. Collectively, these data suggest that the expression of molecules related to the proteolytic machinery is enhanced by PF treatment, which results in a heightened pharmacological effect. The expression of mutant AR is reduced, and the polyQ-dependent phenotype is mitigated by PF in the mouse model of SBMA.

DISCUSSION

Our results demonstrated that mutant AR is sensitive to PF treatment and that the PF-mediated downregulation of mutant AR can ameliorate motor abnormalities in an SBMA mouse model without detectable toxicity. PF treatment reduced the levels of

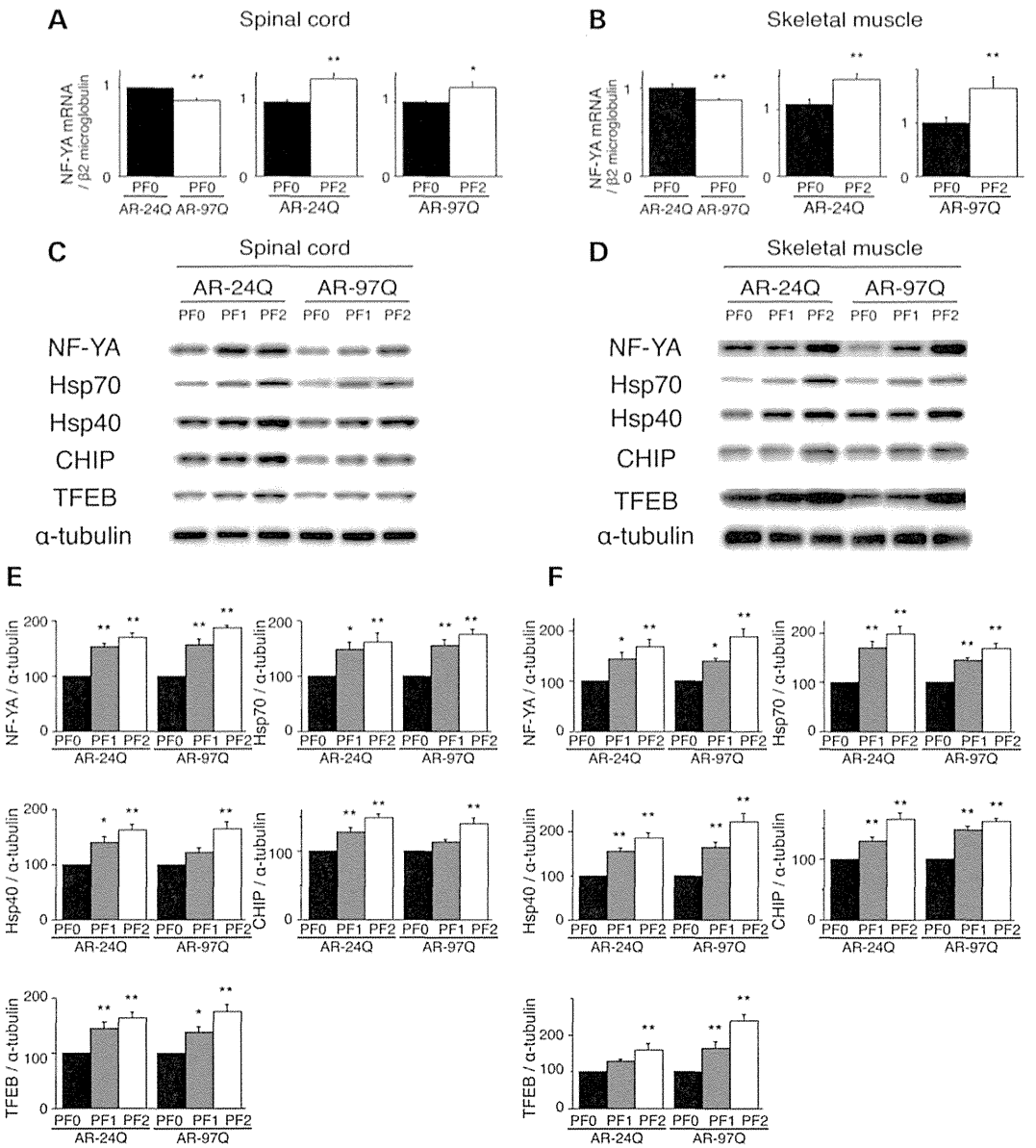

Figure 6. PF increased the expression of molecular chaperones, CHIP and transcription factors in AR-24Q mice and AR-97Q mice. The expression levels of NF-YA mRNA in the spinal cord (**A**) and skeletal muscle (**B**) of 16-week-old AR-24Q mice and AR-97Q mice ($^{**}P < 0.01$; $^{***}P < 0.001$, $n = 5$, unpaired *t*-test). Western blots and densitometric analyses of NF-YA, molecular chaperones, CHIP and TFEB in the spinal cord (**C** and **E**) and skeletal muscle (**D** and **F**) of 16-week-old AR-24Q mice and AR-97Q mice ($^{*}P < 0.05$; $^{**}P < 0.01$, $n = 5$, one-way ANOVA with Tukey–Kramer *post hoc* test). Error bars (A, B, E, F), SEM.

monomeric and aggregated forms of mutant AR. In chronic neurodegenerative disorders, such as polyQ diseases, Parkinson's disease, Alzheimer disease and amyotrophic lateral sclerosis, commonly observed phenotypes include the abnormal accumulation of disease-causing proteins and the formation of nuclear and cytoplasmic inclusions. Under pathologic conditions, the accumulated levels of misfolded and toxic proteins may exceed the protective ability of the proteolytic machinery; the inability to either maintain misfolded proteins in a soluble form or degrade them results in their accumulation and the formation of inclusions. In this study, we showed that PF potently induced a novel, NF-YA-mediated mechanism involving both the UPS and autophagy systems, which downregulated mutant AR accumulation and thereby ameliorated SBMA phenotypes in a mouse model. Motor neuron degeneration induced by mutant AR involves several distinct mechanisms, including transcriptional dysregulation, aggregate formation, impaired axonal transport, DNA binding and mitochondrial dysfunction. Although it remains unclear which of these mechanisms has a pivotal impact on SBMA pathogenesis, the accumulation of mutant AR is a well-established upstream molecular event of neuro- and myodegeneration (3). The successful anti-androgen

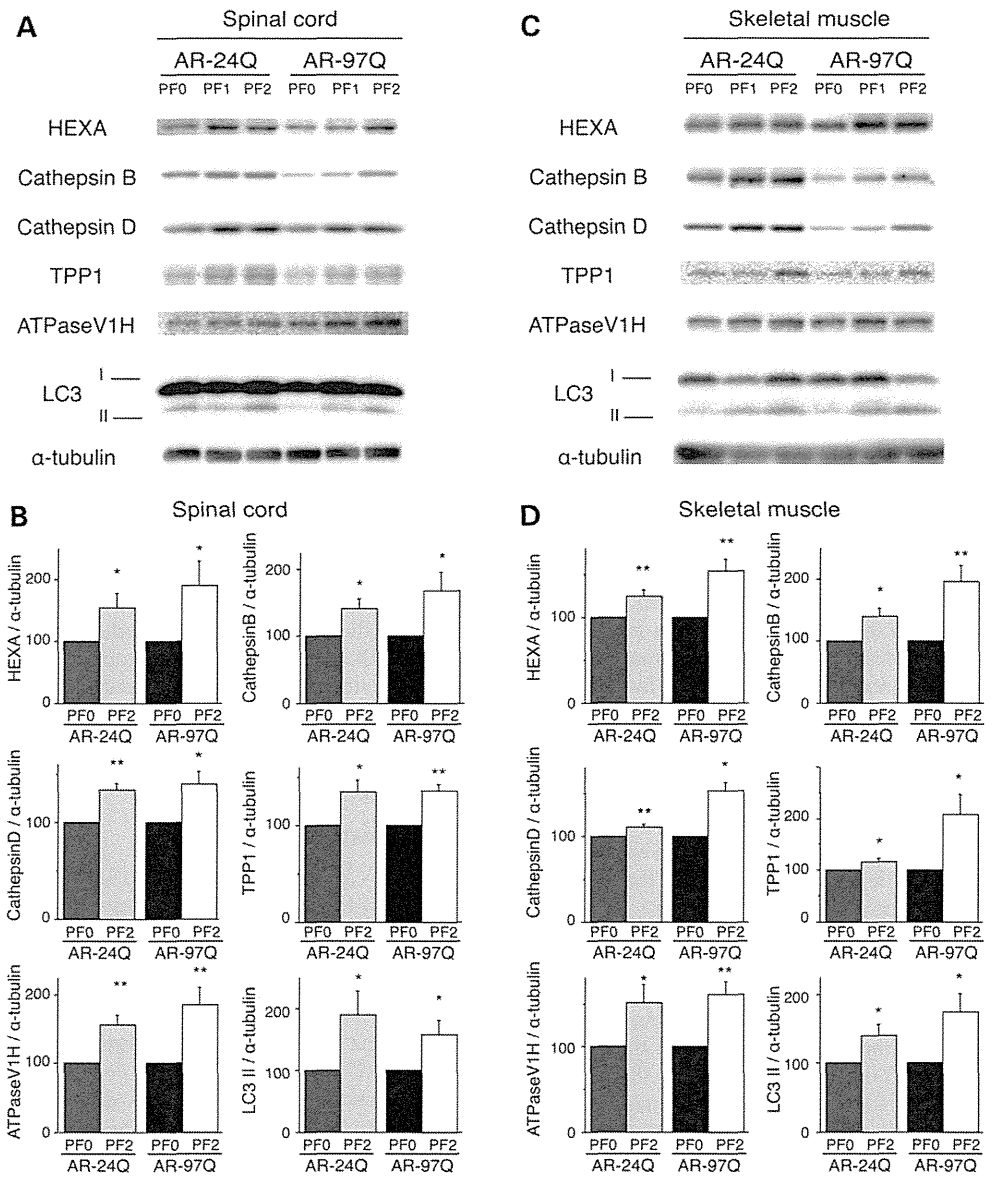

Figure 7. PF increased the expression of lysosomal proteases and LC3-II in AR-24Q and AR-97Q mice. Western blots and densitometric analyses for lysosomal proteases in the spinal cord (**A** and **B**) and skeletal muscle (**C** and **D**) of 16-week-old AR-24Q mice and AR-97Q mice (*$P < 0.05$; **$P < 0.01$, $n = 5$, unpaired t-test). Error bars (B, D), SEM.

therapy in SBMA mouse models has translated to clinical trials, which showed that swallowing function improved in patients with a disease duration of <10 years (24,25). Many studies have sought to elucidate the pathogenesis of polyQ diseases and develop treatment methods. Among these treatments, the pharmacologic induction of molecular chaperones, the UPS and autophagy may ameliorate these disorders (26). The mutant polyQ AR adopts an altered conformation that results in protein aggregation and inclusion formation; however, recent studies have suggested that soluble forms of the causative protein, including oligomeric protein, aggregate. Mutant monomers in the nuclear space may also be toxic (rather than protein inclusions). Thus, soluble protein aggregates, or possibly mutant monomers, represent targets in the treatment of neurodegenerative disorders (27–29). Indeed, we have demonstrated that reducing the levels of the pathogenic AR protein in SBMA mice attenuates the expression of the disease (30–35), which suggests that the clearance of mutant AR may therapeutically benefit SBMA. Our present data also confirm that PF passes through the blood–brain barrier and that long-term treatment with PF exerts significant pharmacological effects in the central nervous system.

NF-Y is a heterotrimeric complex that consists of three subunits, NF-YA, NF-YB and NF-YC, and binds to CCAAT motifs in

the promoter regions of a variety of genes (18). NF-YA was reported to upregulate the expression of molecular chaperones. Our results demonstrate that NF-YA is also able to induce the expression of CHIP and TFEB, which suggests that NF-YA plays a pivotal role in the clearance of pathogenic proteins and the maintenance of proteostasis. The upregulation of diverse molecules involved in the proteolytic machinery must contribute to the marked beneficial effects of PF treatment in the AR-97Q mice. AR-97Q transgene expression decreased the expression of NF-YA, due to the decrease in mRNA levels (Fig. 6A and B) and sequestration of endogenous NF-YA in the inclusions (Supplemental Material, Fig. S6A and B). Consequently, the expression levels of molecular chaperones, CHIP and TFEB decreased in the spinal cord and muscle (Fig. 6C and D). The reduction of these molecules can impair the function of the proteolytic machinery and enhance polyQ toxicity. NF-YA also colocalized with mutant AR NIs that were present in the motor neurons and muscles of SBMA patients (Supplementary Material, Fig. S6A and B). NIs that were positive for NF-YA have been identified in models of SBMA (36), Huntington's disease (HD) (37) and spinocerebellar ataxia 17 (SCA17) (38), which suggests that NF-YA is a protein targeted for sequestration in polyQ diseases. Collectively, these data suggest that PF can increase the expression of NF-YA and restore the proteolytic machinery. It is likely that the proteolytic machinery is inhibited by misfolded proteins in the affected tissues of diverse polyQ diseases, such as SBMA, HD and SCA17 (36–38).

Mutant AR was preferentially degraded compared with wild-type AR in the presence of PF in both the cell culture and mouse models of SBMA. Mutant AR elimination was mediated by the upregulation of molecular chaperones and CHIP in which it was then prone to proteasomal degradation (39). Hsp70 and Hsp40 suppress aggregate formation and cellular toxicity in a wide range of polyQ disease models (30,40–43). CHIP interacts with Hsp90 or Hsp70 and ubiquitinates and degrades unfolded proteins trapped by molecular chaperones (44). A wide variety of proteins have been identified as CHIP substrates, including polyQ disease-causative proteins (45). Unfolded mutant proteins are more efficiently ubiquitinated by CHIP in the presence of molecular chaperones (12). Furthermore, mutant AR with a longer polyQ length is more efficiently ubiquitinated by CHIP (46). Based on these findings, the upregulation of CHIP expression by PF treatment may facilitate the preferential degradation of mutant AR in close cooperation with upregulated molecular chaperones.

Our experiments demonstrated that PF elevated the expression of TFEB and promoted the degradation of ARs via the activation of the autophagy system. AR has been demonstrated to be a direct target of autophagy (47,48). TFEB is a master regulator of lysosomal biogenesis and function (14) and upregulates lysosomal pathways and autophagy by modulating the expression of lysosomal enzymes involved in protein degradation (15). TFEB also regulates lysosomal proteostasis (49) and exocytosis (50). Importantly, TFEB regulates the clearance of disease-causing proteins, including huntingtin (14) and Aβ (51), and its overexpression reduces the expression level of polyQ-expanded huntingtin protein (52). However, chronically enhanced autophagy contributed to the detrimental consequences in the skeletal muscle of an SBMA mouse model (53). Although future studies should weigh the detrimental effects of chronically inducing autophagy to address proteinopathies against our observation of beneficially elevated autophagy in SBMA, sufficient inhibition of AR accumulation may overcome the deleterious effects of autophagy induction on muscle atrophy. Overall, based on our observations and taking the results from the previous studies into account, PF treatment promoted the degradation of both wild-type and mutant ARs by activating lysosomal biogenesis via the TFEB pathway and thereby restored the phenotypic defects in the SBMA mouse model. Collectively, PF treatment could provide a two-pronged cooperative therapeutic effect against SBMA pathogenesis by activating the molecular chaperone–UPS system and the autophagy system to degrade the mutant AR.

In conclusion, our present study demonstrated the safety and efficacy of PF in a mouse model of SBMA. PF potently induced the proteolytic machinery of UPS and autophagy, which lead to mutant AR degradation. In SBMA patients, the diffuse nuclear accumulation of mutant AR is frequent and extensive and occurs both in regions of the central nervous system and in muscles. The accumulation of pathogenic proteins causes many age-related neurodegenerative diseases. Inducers of the proteolytic machinery appear to be potent agents for disease-modifying therapies that inhibit the pathogenic process of neuron degeneration (54); thus, the pharmacological induction of the proteolytic machinery through PF treatment appears to be an applicable therapeutic strategy for multiple neurodegenerative disorders, including SBMA.

MATERIALS AND METHODS

Plasmid constructs and siRNA

pcDNA3.1/V5-His-NF-YA plasmid (37) was kindly provided by Dr Nobuyuki Nukina in the Department of Neuroscience for Neurodegenerative Disorders, Juntendo University Graduate School of Medicine. The plasmids pCR3.1-AR-24Q and pCR3.1-AR-97Q (32) were also used. The human TFEB cDNA was cloned into pcDNA 6.2/V5-GW/D-TOPO (Invitrogen) from the RNA of SH-SY5Y human neuroblastoma cells (ATCC No. CRL-2266). All of the constructs were verified by DNA sequencing. For the knock-down of NF-YA, 10 nM siRNA was used with the following sequence: 5′-CAGUAUCA CACCGCAUCCUUATT-3′ (sense) and 5′-UAAGGAUGCGG UGAUACUGTT-3′ (anti-sense). We used MISSION siRNA Universal Negative Control (Sigma) as the control siRNA.

Cell culture and DNA transfection

NSC34 cells were transfected using Lipofectamine 2000 (Invitrogen, Carlsbad, CA, USA) with plasmids encoding ARs containing normal (24 CAGs) or expanded (97 CAGs) polyQ repeats (32). Stable clones expressing these normal and mutant ARs were established by selection with the antibiotic G418 (0.4 mg/ml final concentration). The AR is not expressed in non-transfected NSC34 cells. All cell cultures were propagated in the absence of androgen. In western blots from these cultures, we detected a band of monomeric mutant AR in the separating gel but could hardly detect the high-molecular-weight mutant AR protein complex, which was retained in the stacking gel. Therefore, this cultured cell model is better suited for estimating the change in monomeric mutant AR expression.

Wild-type Neuro2A cells or NSC34 cells and NSC34 cells stably expressing the human AR24Q or AR97Q were plated in six-well dishes in 5 ml of DMEM/10% fetal bovine serum (FBS) (Dulbecco's modified Eagle's medium supplemented with 10% FBS) with penicillin and streptomycin. Each dish was transfected with 4 μg of DNA plasmids and siRNA or control (mock) using Lipofectamine 2000 (Invitrogen) according to the manufacturer's instructions. NSC34 cells were cultured in differentiation medium (DMEM/2% FBS) containing dihydrotestosterone (DHT; 1 nM) after transfection. The transfection efficiency was 60–70%. Neuro2A cells were cultured in differentiation medium (DMEM/2% FBS) containing retinoic acid (20 μM) and DHT (1 nM) after transfection. The transfection efficiency was 60–70%.

Promoter assay

GoClone and the pGL4 Luciferase Reporter Vector encoding the NF-YA, TFEB, Hsp70 and CHIP promoter (SwitchGear Genomics) were transfected into NSC34 cells with Lipofectamine 2000 (Invitrogen). The Steady-Glo Luciferase Assay System (Promega) was used to measure expression with POWERSCAN 4 (DS Pharma Biomedical).

Generation and maintenance of transgenic mice

We used AR-24Q and AR-97Q male mice in this study (21). The AR-97Q (Line #7–8) male mice showed progressive muscular atrophy and weakness accompanied by diffuse nuclear staining and NIs of the mutant AR. Similar to SBMA patients, these phenotypes were very pronounced in the male transgenic mice. The littermates were also used for phenotypic analyses. All of the animal experiments were performed in accordance with the National Institutes of Health Guide for the Care and Use of Laboratory Animals and under the approval of the Nagoya University Animal Experiment Committee.

Therapeutic agents and protocol for administration

PF, purchased from Wako Pure Chemical Industries (Japan) (molecular weight: 480.45, 10 mg), was dissolved in 1 ml of PBS, diluted for use in culture medium and stored in the freezer until use. For the SBMA mouse model, we stored 10 mg/ml stock solutions of PF dissolved in a 0.9% NaCl solution at −20°C. To demonstrate that PF slows the onset and progression of the disease, PF treatments were initiated when the mice reached 5 weeks of age and continued until they were 32 weeks old. The stock solution was diluted to 1 mg/ml with saline solution just before the experiment, and 6.7 or 13.4 mg/kg of PF was administered intraperitoneally every day. The control mice received saline.

Neurological and behavioral assessments of the SBMA mouse model

Mice of varying ages were assessed with two different behavioral tests by investigators blind to the genotype and treatment. The rotarod task (Ugo Basile) was performed on a weekly basis, and cage activity was measured weekly with the AB system (Neuroscience) (21). Spontaneous motor activity was monitored for periods of 24 h; all spontaneous movements, both vertical and horizontal, including locomotion, rearing and head movements, were counted and automatically totaled.

Immunohistochemistry and histopathology

Mice were deeply anesthetized with pentobarbital sodium. The spinal cord and skeletal muscle tissues were removed, fixed overnight in 10% phosphate-buffered formalin and processed for paraffin embedding. Sections (6 μM thick) of tissue were deparaffinized, dehydrated with alcohol and treated in formic acid for 5 min at room temperature. For the immunohistochemical studies, the paraffin sections were preheated in a microwave oven for 10 min and blocked with normal animal serum (1:20). The sections were then incubated with anti-expanded polyQ antibody (1:10 000; 1C2; Millipore), anti-NF-YA antibody (1:1000; H-209; Santa Cruz), anti-TFEB antibody (1:1000; Medical and Biological Laboratories) and anti-GFAP antibody (1:1000; Roche Diagnostics). The primary antibodies were probed with a biotinylated anti-species-specific IgG (Vector), and the immune complexes were visualized using streptavidin–horseradish peroxidase (HRP) (Dako) and 3,3-diaminobenzidine (Dojindo) as a substrate. The sections were counterstained with Mayer's hematoxylin. Paraffin-embedded sections (6 μm thick) of the gastrocnemius muscles were air-dried and stained with hematoxylin and eosin. For double-immunofluorescence staining, the sections were blocked with TSA Blocking Reagent (PerkinElmer) and then sequentially incubated with anti-NF-YA antibody (1:1000; H-209; Santa Cruz) and 1C2 antibody (1:10000; Millipore) at 4°C overnight. The sections were then incubated with Alexa 488-conjugated goat anti-rabbit IgG (1:1000; Invitrogen) and Alexa 546-conjugated goat anti-mouse IgG (1:1300; Invitrogen) for 8 h at 4°C. The stained sections were examined and imaged with a confocal laser-scanning microscope (LSM 710; Carl Zeiss).

Patients

Tissue was obtained from three patients with clinicopathologically and genetically confirmed SBMA (51–77 years of age; mean, 65.7 years) and three non-neurological controls (51–78 years of age; mean, 64.0 years). The patients were hospitalized and evaluated at Nagoya University Hospital and affiliated hospitals. The collection of human tissues and their use for this study were approved by the Ethics Committee of Nagoya University Graduate School of Medicine. Informed consent was obtained to use the tissues for research purposes. Paraffin-embedded sections of the spinal cord were processed and examined in the same manner as those of the transgenic mice.

Quantification of 1C2-positive cells

To assess 1C2-positive cells in the ventral horn of the spinal cord, 50 consecutive transverse sections of the thoracic spinal cord were prepared from each individual mouse. 1C2-positive cells within the ventral horn of every fifth section were counted (55). Populations of 1C2-positive cells were expressed as the number/mm^2 (Fig. 5B). To examine 1C2-positive cells in the muscle, the number of 1C2-positive cells was calculated from counts of 500 fibers in randomly selected areas and expressed

as the number per 100 muscle fibers (Fig. 5B). The quantitative data of six individual mice were expressed as the mean ± SEM.

Protein expression analysis

Forty-eight hours after transfection, the cells were lysed in CelLytic-M Mammalian Cell Lysis/Extraction Reagent (Sigma), supplemented with 1 mM phenylmethylsulfonyl fluoride (PMSF) and 6 μg/ml aprotinin and centrifuged at 1000*g* for 15 min at 4°C. NE-PER Nuclear Cytoplasmic Reagents (Thermo Scientific) were used for the analysis of the nuclear/cytoplasmic translocation of TFEB. Sixteen-week-old mice were exsanguinated under pentobarbital sodium anesthesia, and the tissues were snap-frozen with powdered CO_2 in acetone. The tissues were homogenized in CelLytic-M Mammalian Cell Lysis/Extraction Reagent with 1 mM PMSF and 6 μg/ml aprotinin and centrifuged at 2500*g* for 15 min at 4°C. The supernatant protein concentrations were determined using the DC protein assay (Bio-Rad). Aliquots of the supernatant fractions were loaded on 5–20% SDS–PAGE gels, where each lane contained 7 μg of cell protein and 40 μg of neural and muscle tissue. The gels were then transferred to Hybond-P membranes (GE Healthcare) using transfer buffer (25 mM Tris, 192 mM glycine, 0.1% SDS, 10% methanol). The following antibodies were used in our studies: anti-AR (1:1000; N20; Santa Cruz), anti-AR (1:1000; H280; Santa Cruz), anti-NF-YA (1:1000; H-209; Santa Cruz), anti-TFEB (1:5000; ab2636; Abcam), anti-HSP70 (1:10 000; SPA-810; Enzo Life Sciences), anti-HSP70 (1:1000; #4872; Cell Signaling Technology), anti-HSP40 (1:10 000; SPA-400; Enzo Life Sciences), anti-HSP40 (1:1000; #4868; Cell Signaling Technology), anti-CHIP (1:1000; #C3B6; Cell Signaling Technology), mouse anti-GAPDH (1:10000; MAB374; Millipore), mouse anti-α-tubulin (1:5000, T9026; Sigma), anti-LC3 (1:1000; #D11; Cell Signaling Technology), anti-V5 (1:5000; PM003; Medical & Biological Laboratories), anti-hexosaminidase A (1:1000; N-19; Santa Cruz), anti-Cathepsin B (1:2000; ab33538; Abcam), anti-Cathepsin D (1:2000; ab6313; Abcam), anti-tripeptidyl peptidase 1 (1:1000; G-16; Santa Cruz), anti-V-ATPase H (1:2000; H-300; Santa Cruz), anti-mTOR (1:2000; #2983; Cell Signaling Technology), anti-Phospho-mTOR (1:2000; #2974; Cell Signaling Technology), anti-p70 S6 Kinase (1:2000; #2708; Cell Signaling Technology), anti-Phospho-p70 S6 Kinase (1:2000; #9234; Cell Signaling Technology), anti-eukaryotic initiation factor 4E-binding protein 1 (4E-BP1) (1:2000; #9644; Cell Signaling Technology), anti-Phospho-4E-BP1 (Thr37/46; 1:2000; #2855; Cell Signaling Technology) and anti-Beclin-1 (1:2000; #3495; Cell Signaling Technology). The primary antibodies were probed using HRP-conjugated anti-rabbit IgG F(ab′)2 and anti-mouse IgG F(ab′)2 (1:5000; GE Healthcare) secondary antibodies and were detected with the ECL Prime kit (GE Healthcare). An LAS-3000 imaging system was used to produce digital images and to quantify the band intensities, which were then analyzed with the Image Gauge software version 4.22 (Fujifilm). Densitometric values of ARs were normalized to endogenous GAPDH.

Pulse-chase labeling assay

NSC34 cells stably expressing the human AR24Q or AR97Q were plated in 6-cm dishes in 5 ml of DMEM/10% FBS containing DHT (1 nM) supplemented with penicillin and streptomycin. Each dish was treated with 10 μM of PF or PBS as a control. The cells were starved for 1 h in methionine- and cysteine-free DMEM/10% FBS and then labeled for 1 h with 150 Ci/ml of Redivue Pro-Mix L-[35S] *in vitro* cell-labeling mix (GE Healthcare). After washing in PBS, the cells were chased for the indicated time intervals in complete medium containing 10 μM of PF or saline. PF-treated cells were also treated with 20 nM bafilomycin A1 (11707; Sigma) or 2.5 μM lactacystin (PEPTIDE INSTITUTE, Inc.). Immunoprecipitation was performed using equivalent amounts of protein lysates, 50 μl of protein G Dynabeads (Invitrogen) and 5 μl of anti-AR antibody (N20; Santa Cruz) for 10 min at room temperature. Each sample was separated by 5–20% SDS–PAGE and analyzed by phosphorimaging (Typhoon LFA 9000 PhosphorImager; GE Healthcare) and Image Gauge software version 4.22 (Fujifilm).

Quantitative real-time reverse transcription–PCR

Total RNA was isolated from the NSC34 cells using the RNeasy Mini kit (Qiagen) and from mouse tissues using the PureLink RNA Mini kit (Invitrogen) according to the manufacturer's instructions. Total RNA from cells (3 μg) and mouse tissues (2.5 μg) was transcribed using the SuperScript VILO cDNA Synthesis Kit (Invitrogen). Real-time RT–PCR was performed in a total volume of 25 μl containing 12.5 μl of 2× QuantiFast SYBR Green PCR Master Mix (Qiagen) and 1 μM of each primer. The PCR products were detected by the iCycler system (Bio-Rad). The reaction conditions were 95°C for 5 min, 40 cycles of 10 s at 95°C and 30 s at 60°C. As an internal standard control, the expression level of β2 microglobulin was simultaneously quantified. The primer sequences are listed in Supplementary Material, Table S1.

Cell viability assay

The 3-(4,5-dimethylthiazol-2-yl)-5-(3-carboxymethoxyphenyl)-2-(4-sulfophenyl)-2H-tetrazolium, inner salt (MTS)-based cell proliferation assay was performed in triplicate in NSC34 cells stably expressing the human AR24Q or AR97Q using the Cell Proliferation Reagent WST-1 (Roche Applied Science) and the CellTiter 96® AQueous One Solution Cell Proliferation Assay (Promega) 48 h after incubation with PF.

Serum testosterone assay

Mice receiving PF or saline were deeply anesthetized with pentobarbital sodium at 16 weeks of age, 1 ml of blood was collected by cardiocentesis, and serum testosterone was assayed with the Coat-A-Count Total Testosterone radioimmunoassay (Roche) according to the manufacturer's instructions.

Statistical analysis

The data were analyzed using unpaired *t*-tests and *post hoc* tests (Tukey–Kramer *post hoc* tests) for multiple comparisons. The Kaplan–Meier and log-rank tests were used to assess the survival rate using StatView software version 5 (Hulinks).

SUPPLEMENTARY MATERIAL

Supplementary Material is available at *HMG* online.

ACKNOWLEDGEMENTS

We thank Miwa Ito and Kazuko Matsuba in the Department of Neurology and Yasutaka Ohya and Kumiko Yano in the Division for Research of Laboratory Animals at the Center for Research of Laboratory Animals and Medical Research Engineering for their technical assistance. We also thank Dr Nobuyuki Nukina in the Department of Neuroscience for Neurodegenerative Disorders, Juntendo University Graduate School of Medicine, for kindly providing the vectors containing NF-YA.

Conflict of Interest statement. None declared.

FUNDING

This work was supported by a Center-of-Excellence (COE) grant, KAKENHI (20390243) and additional grants from the Ministry of Education, Culture, Sports, Science and Technology of Japan.

REFERENCES

1. Di Prospero, N.A. and Fischbeck, K.H. (2005) Therapeutics development for triplet repeat expansion diseases. *Nat. Rev. Genet.*, **6**, 756–765.
2. Adachi, H., Waza, M., Katsuno, M., Tanaka, F., Doyu, M. and Sobue, G. (2007) Pathogenesis and molecular targeted therapy of spinal and bulbar muscular atrophy. *Neuropathol. Appl. Neurobiol.*, **33**, 135–151.
3. Adachi, H., Katsuno, M., Minamiyama, M., Waza, M., Sang, C., Nakagomi, Y., Kobayashi, Y., Tanaka, F., Doyu, M., Inukai, A. *et al.* (2005) Widespread nuclear and cytoplasmic accumulation of mutant androgen receptor in SBMA patients. *Brain*, **128**, 659–670.
4. Sobue, G., Hashizume, Y., Mukai, E., Hirayama, M., Mitsuma, T. and Takahashi, A. (1989) X-linked recessive bulbospinal neuronopathy. A clinicopathological study. *Brain*, **112**, 209–232.
5. Soraru, G., D'Ascenzo, C., Polo, A., Palmieri, A., Baggio, L., Vergani, L., Gellera, C., Moretto, G., Pegoraro, E. and Angelini, C. (2008) Spinal and bulbar muscular atrophy: skeletal muscle pathology in male patients and heterozygous females. *J. Neurol. Sci.*, **264**, 100–105.
6. Atsuta, N., Watanabe, H., Ito, M., Banno, H., Suzuki, K., Katsuno, M., Tanaka, F., Tamakoshi, A. and Sobue, G. (2006) Natural history of spinal and bulbar muscular atrophy (SBMA): a study of 223 Japanese patients. *Brain*, **129**, 1446–1455.
7. Rhodes, L.E., Freeman, B.K., Auh, S., Kokkinis, A.D., La Pean, A., Chen, C., Lehky, T.J., Shrader, J.A., Levy, E.W., Harris-Love, M. *et al.* (2009) Clinical features of spinal and bulbar muscular atrophy. *Brain*, **132**, 3242–3251.
8. Buchberger, A., Bukau, B. and Sommer, T. (2010) Protein quality control in the cytosol and the endoplasmic reticulum: brothers in arms. *Mol. Cell*, **40**, 238–252.
9. Adachi, H., Katsuno, M., Waza, M., Minamiyama, M., Tanaka, F. and Sobue, G. (2009) Heat shock proteins in neurodegenerative diseases: pathogenic roles and therapeutic implications. *Int. J. Hyperthermia*, **25**, 647–654.
10. Labbadia, J., Cunliffe, H., Weiss, A., Katsyuba, E., Sathasivam, K., Seredenina, T., Woodman, B., Moussaoui, S., Frentzel, S., Luthi-Carter, R. *et al.* (2011) Altered chromatin architecture underlies progressive impairment of the heat shock response in mouse models of Huntington disease. *J. Clin. Invest.*, **121**, 3306–3319.
11. Bailey, C.K., Andriola, I.F., Kampinga, H.H. and Merry, D.E. (2002) Molecular chaperones enhance the degradation of expanded polyglutamine repeat androgen receptor in a cellular model of spinal and bulbar muscular atrophy. *Hum. Mol. Genet.*, **11**, 515–523.
12. Stankiewicz, M., Nikolay, R., Rybin, V. and Mayer, M.P. (2010) CHIP participates in protein triage decisions by preferentially ubiquitinating Hsp70-bound substrates. *FEBS J*, **277**, 3353–3367.
13. Kabeya, Y., Mizushima, N., Ueno, T., Yamamoto, A., Kirisako, T., Noda, T., Kominami, E., Ohsumi, Y. and Yoshimori, T. (2000) LC3, a mammalian homologue of yeast Apg8p, is localized in autophagosome membranes after processing. *EMBO J.*, **19**, 5720–5728.
14. Sardiello, M., Palmieri, M., di Ronza, A., Medina, D.L., Valenza, M., Gennarino, V.A., Di Malta, C., Donaudy, F., Embrione, V., Polishchuk, R.S. *et al.* (2009) A gene network regulating lysosomal biogenesis and function. *Science*, **325**, 473–477.
15. Settembre, C., Di Malta, C., Polito, V.A., Garcia Arencibia, M., Vetrini, F., Erdin, S., Erdin, S.U., Huynh, T., Medina, D., Colella, P. *et al.* (2011) TFEB links autophagy to lysosomal biogenesis. *Science*, **332**, 1429–1433.
16. Yan, D., Saito, K., Ohmi, Y., Fujie, N. and Ohtsuka, K. (2004) Paeoniflorin, a novel heat shock protein-inducing compound. *Cell Stress Chaperones*, **9**, 378–389.
17. Sun, X., Cao, Y.B., Hu, L.F., Yang, Y.P., Li, J., Wang, F. and Liu, C.F. (2011) ASICs mediate the modulatory effect by paeoniflorin on alpha-synuclein autophagic degradation. *Brain Res.*, **1396**, 77–87.
18. Dolfini, D., Gatta, R. and Mantovani, R. (2012) NF-Y and the transcriptional activation of CCAAT promoters. *Crit. Rev. Biochem. Mol. Biol.*, **47**, 29–49.
19. Lee, L.C., Chen, C.M., Wang, H.C., Hsieh, H.H., Chiu, I.S., Su, M.T., Hsieh-Li, H.M., Wu, C.H., Lee, G.C., Lee-Chen, G.J. *et al.* (2012) Role of the CCAAT-binding protein NFY in SCA17 pathogenesis. *PLoS ONE*, **7**, e35302.
20. Lieberman, A.P., Harmison, G., Strand, A.D., Olson, J.M. and Fischbeck, K.H. (2002) Altered transcriptional regulation in cells expressing the expanded polyglutamine androgen receptor. *Hum. Mol. Genet.*, **11**, 1967–1976.
21. Katsuno, M., Adachi, H., Kume, A., Li, M., Nakagomi, Y., Niwa, H., Sang, C., Kobayashi, Y., Doyu, M. and Sobue, G. (2002) Testosterone reduction prevents phenotypic expression in a transgenic mouse model of spinal and bulbar muscular atrophy. *Neuron*, **35**, 843–854.
22. Kondo, N., Katsuno, M., Adachi, H., Minamiyama, M., Doi, H., Matsumoto, S., Miyazaki, Y., Iida, M., Tohnai, G., Nakatsuji, H. *et al.* (2013) Heat shock factor-1 influences pathological lesion distribution of polyglutamine-induced neurodegeneration. *Nat. Commun.*, **4**. doi: 10.1038/ncomms2417.
23. Tagawa, K., Marubuchi, S., Qi, M.L., Enokido, Y., Tamura, T., Inagaki, R., Murata, M., Kanazawa, I., Wanker, E.E. and Okazawa, H. (2007) The induction levels of heat shock protein 70 differentiate the vulnerabilities to mutant huntingtin among neuronal subtypes. *J. Neurosci.*, **27**, 868–880.
24. Katsuno, M., Banno, H., Suzuki, K., Takeuchi, Y., Kawashima, M., Yabe, I., Sasaki, H., Aoki, M., Morita, M. and Nakano, I. (2010) Efficacy and safety of leuprorelin in patients with spinal and bulbar muscular atrophy (JASMITT study): a multicentre, randomised, double-blind, placebo-controlled trial. *Lancet Neurol.*, **9**, 875–884.
25. Fernandez-Rhodes, L.E., Kokkinis, A.D., White, M.J., Watts, C.A., Auh, S., Jeffries, N.O., Shrader, J.A., Lehky, T.J., Li, L., Ryder, J.E. *et al.* (2011) Efficacy and safety of dutasteride in patients with spinal and bulbar muscular atrophy: a randomised placebo-controlled trial. *Lancet Neurol.*, **10**, 140–147.
26. Parodi, S. and Pennuto, M. (2011) Neurotoxic effects of androgens in spinal and bulbar muscular atrophy. *Front. Neuroendocrinol.*, **32**, 416–425.
27. Hands, S.L. and Wyttenbach, A. (2010) Neurotoxic protein oligomerisation associated with polyglutamine diseases. *Acta Neuropathol.*, **120**, 419–437.
28. Naiki, H. and Nagai, Y. (2009) Molecular pathogenesis of protein misfolding diseases: pathological molecular environments versus quality control systems against misfolded proteins. *J. Biochem.*, **146**, 751–756.
29. Bauer, P.O. and Nukina, N. (2009) The pathogenic mechanisms of polyglutamine diseases and current therapeutic strategies. *J. Neurochem.*, **110**, 1737–1765.
30. Adachi, H., Katsuno, M., Minamiyama, M., Sang, C., Pagoulatos, G., Angelidis, C., Kusakabe, M., Yoshiki, A., Kobayashi, Y., Doyu, M. *et al.* (2003) Heat shock protein 70 chaperone overexpression ameliorates phenotypes of the spinal and bulbar muscular atrophy transgenic mouse model by reducing nuclear-localized mutant androgen receptor protein. *J. Neurosci.*, **23**, 2203–2211.
31. Katsuno, M., Adachi, H., Doyu, M., Minamiyama, M., Sang, C., Kobayashi, Y., Inukai, A. and Sobue, G. (2003) Leuprorelin rescues polyglutamine-dependent phenotypes in a transgenic mouse model of spinal and bulbar muscular atrophy. *Nat. Med.*, **9**, 768–773.

32. Waza, M., Adachi, H., Katsuno, M., Minamiyama, M., Sang, C., Tanaka, F., Inukai, A., Doyu, M. and Sobue, G. (2005) 17-AAG, an Hsp90 inhibitor, ameliorates polyglutamine-mediated motor neuron degeneration. *Nat. Med.*, **11**, 1088–1095.
33. Yang, Z., Chang, Y.J., Yu, I.C., Yeh, S., Wu, C.C., Miyamoto, H., Merry, D.E., Sobue, G., Chen, L.M., Chang, S.S. *et al.* (2007) ASC-J9 ameliorates spinal and bulbar muscular atrophy phenotype via degradation of androgen receptor. *Nat. Med.*, **13**, 348–353.
34. Miyazaki, Y., Adachi, H., Katsuno, M., Minamiyama, M., Jiang, Y.M., Huang, Z., Doi, H., Matsumoto, S., Kondo, N., Iida, M. *et al.* (2012) Viral delivery of miR-196a ameliorates the SBMA phenotype via the silencing of CELF2. *Nat. Med.*, **18**, 1136–1141.
35. Rinaldi, C., Bott, L.C., Chen, K.L., Harmison, G.G., Katsuno, M., Sobue, G., Pennuto, M. and Fischbeck, K.H. (2012) Insulinlike growth factor (IGF)-1 administration ameliorates disease manifestations in a mouse model of spinal and bulbar muscular atrophy. *Mol. Med.*, **18**, 1261–1268.
36. Katsuno, M., Adachi, H., Minamiyama, M., Waza, M., Doi, H., Kondo, N., Mizoguchi, H., Nitta, A., Yamada, K., Banno, H. *et al.* (2010) Disrupted transforming growth factor-beta signaling in spinal and bulbar muscular atrophy. *J. Neurosci.*, **30**, 5702–5712.
37. Yamanaka, T., Miyazaki, H., Oyama, F., Kurosawa, M., Washizu, C., Doi, H. and Nukina, N. (2008) Mutant Huntingtin reduces HSP70 expression through the sequestration of NF-Y transcription factor. *EMBO J.*, **27**, 827–839.
38. Huang, S., Ling, J.J., Yang, S., Li, X.J. and Li, S. (2011) Neuronal expression of TATA box-binding protein containing expanded polyglutamine in knock-in mice reduces chaperone protein response by impairing the function of nuclear factor-Y transcription factor. *Brain*, **134**, 1943–1958.
39. Wang, A.M., Miyata, Y., Klinedinst, S., Peng, H.M., Chua, J.P., Komiyama, T., Li, X., Morishima, Y., Merry, D.E., Pratt, W.B. *et al.* (2013) Activation of Hsp70 reduces neurotoxicity by promoting polyglutamine protein degradation. *Nat. Chem. Biol.*, **9**, 112–118.
40. Cummings, C.J., Sun, Y., Opal, P., Antalffy, B., Mestril, R., Orr, H.T., Dillmann, W.H. and Zoghbi, H.Y. (2001) Over-expression of inducible HSP70 chaperone suppresses neuropathology and improves motor function in SCA1 mice. *Hum. Mol. Genet.*, **10**, 1511–1518.
41. Labbadia, J., Novoselov, S.S., Bett, J.S., Weiss, A., Paganetti, P., Bates, G.P. and Cheetham, M.E. (2012) Suppression of protein aggregation by chaperone modification of high molecular weight complexes. *Brain*, **135**, 1180–1196.
42. Malik, B., Nirmalananthan, N., Gray, A.L., La Spada, A.R., Hanna, M.G. and Greensmith, L. (2013) Co-induction of the heat shock response ameliorates disease progression in a mouse model of human spinal and bulbar muscular atrophy: implications for therapy. *Brain*, **136**, 926–943.
43. Popiel, H.A., Takeuchi, T., Fujita, H., Yamamoto, K., Ito, C., Yamane, H., Muramatsu, S., Toda, T., Wada, K. and Nagai, Y. (2012) Hsp40 gene therapy exerts therapeutic effects on polyglutamine disease mice via a non-cell autonomous mechanism. *PLoS ONE*, **7**, e51069.
44. Murata, S., Minami, Y., Minami, M., Chiba, T. and Tanaka, K. (2001) CHIP is a chaperone-dependent E3 ligase that ubiquitylates unfolded protein. *EMBO Rep.*, **2**, 1133–1138.
45. Miller, V.M., Nelson, R.F., Gouvion, C.M., Williams, A., Rodriguez-Lebron, E., Harper, S.Q., Davidson, B.L., Rebagliati, M.R. and Paulson, H.L. (2005) CHIP suppresses polyglutamine aggregation and toxicity in vitro and in vivo. *J. Neurosci.*, **25**, 9152–9161.
46. Adachi, H., Waza, M., Tokui, K., Katsuno, M., Minamiyama, M., Tanaka, F., Doyu, M. and Sobue, G. (2007) CHIP overexpression reduces mutant androgen receptor protein and ameliorates phenotypes of the spinal and bulbar muscular atrophy transgenic mouse model. *J. Neurosci.*, **27**, 5115–5126.
47. Montie, H.L., Cho, M.S., Holder, L., Liu, Y., Tsvetkov, A.S., Finkbeiner, S. and Merry, D.E. (2009) Cytoplasmic retention of polyglutamine-expanded androgen receptor ameliorates disease via autophagy in a mouse model of spinal and bulbar muscular atrophy. *Hum. Mol. Genet.*, **18**, 1937–1950.
48. Doi, H., Adachi, H., Katsuno, M., Minamiyama, M., Matsumoto, S., Kondo, N., Miyazaki, Y., Iida, M., Tohnai, G., Qiang, Q. *et al.* (2013) p62/SQSTM1 differentially removes thetoxic mutant androgen receptor via autophagy and inclusionformation in a spinal and bulbar muscular atrophy mouse model. *J. Neurosci.*, **33**, 7710–7727.
49. Song, W., Wang, F., Savini, M., Ake, A., di Ronza, A., Sardiello, M. and Segatori, L. (2013) TFEB regulates lysosomal proteostasis. *Hum. Mol. Genet.*, **22**, 1994–2009.
50. Medina, D.L., Fraldi, A., Bouche, V., Annunziata, F., Mansueto, G., Spampanato, C., Puri, C., Pignata, A., Martina, J.A., Sardiello, M. *et al.* (2011) Transcriptional activation of lysosomal exocytosis promotes cellular clearance. *Dev. Cell*, **21**, 421–430.
51. Parr, C., Carzaniga, R., Gentleman, S.M., Van Leuven, F., Walter, J. and Sastre, M. (2012) Glycogen synthase kinase 3 inhibition promotes lysosomal biogenesis and autophagic degradation of the amyloid-beta precursor protein. *Mol. Cell. Biol.*, **32**, 4410–4418.
52. Tsunemi, T., Ashe, T.D., Morrison, B.E., Soriano, K.R., Au, J., Roque, R.A., Lazarowski, E.R., Damian, V.A., Masliah, E. and La Spada, A.R. (2012) PGC-1alpha rescues Huntington's disease proteotoxicity by preventing oxidative stress and promoting TFEB function. *Sci. Transl. Med.*, **4**, 142ra197.
53. Chua, J.P., Reddy, S.L., Merry, D.E., Adachi, H., Katsuno, M., Sobue, G., Robins, D.M. and Lieberman, A.P. (2014) Transcriptional activation of TFEB/ZKSCAN3 target genes underlies enhanced autophagy in spinobulbar muscular atrophy. *Hum. Mol. Genet.*, **23**, 1376–1386.
54. Tanaka, K. and Matsuda, N. (2013) Proteostasis and neurodegeneration: the roles of proteasomal degradation and autophagy. *Biochim. Biophys. Acta.* doi: 10.1016/j.bbamcr.2013.03.012.
55. Adachi, H., Kume, A., Li, M., Nakagomi, Y., Niwa, H., Do, J., Sang, C., Kobayashi, Y., Doyu, M. and Sobue, G. (2001) Transgenic mice with an expanded CAG repeat controlled by the human AR promoter show polyglutamine nuclear inclusions and neuronal dysfunction without neuronal cell death. *Hum. Mol. Genet.*, **10**, 1039–1048.

Articles

High frequency of beta-propeller protein-associated neurodegeneration (BPAN) among patients with intellectual disability and young onset parkinsonism

Kenya Nishioka, MD, PhD[1], Genko Oyama, MD, PhD[1], Hiroyo Yoshino, PhD[2], Yuanzhe Li, MD, PhD[1], Takashi Matsushima MD[1], Chisen Takeuchi MD, PhD[3], Yoko Mochizuki MD, PhD[3], Madoka Mori-Yoshimura, MD, PhD[4], Miho Murata, MD, PhD[4], Chikara Yamasita MD, PhD[5], Norimichi Nakamura MD[5], Yohei Konishi MD, PhD[6], Kazuki Ohi, MD, PhD[7], Keiji Ichikawa, MD[7], Tatsuhiro Terada, MD, PhD[8], Tomokazu Obi, MD, PhD[8], Manabu Funayama PhD[1,2], Shinji Saiki, MD, PhD[1], Nobutaka Hattori, MD, PhD[1,2]

1Department of Neurology, Juntendo University School of Medicine, 2-1-1 Hongo, Bunkyo-ku, Tokyo 113-8421, Japan.

2Research Institute for Diseases of Old Age, Graduate School of Medicine, Juntendo University, 2-1-1 Hongo, Bunkyo-ku, Tokyo 113-8421, Japan.

3Department of Neurology, Tokyo Metropolitan Kita Medical and Rehabilitation Center for the Disabled, 1-2-3 Jyujyodai Kita-ku, Tokyo 114-0033, Japan.

4Department of Neurology, National Centre Hospital, National Centre of Neurology and Psychiatry, 4-1-1 Ogawahigashi, Kodaira, Tokyo 187-8551, Japan.

5Department of Neurology, Kyushu University Hospital, 3-1-1 Maidashi Higashi-ku, Fukuoka 812-8582, Japan.

6Department of Neurology, Yotsukaidou Tokushukai Medical Center, 1830-1 Yoshioka, Yotsukaido, Chiba 284-0032, Japan.

7Department of Neurology, Hyogo Prefectural Amagasaki Hospital, 1-1-1 Higashidaimotsu-cho, Amagasaki, Hyogo 660-0828, Japan.

8Department of Neurology, Shizuoka Institute of Epilepsy and Neurological Disorders, Urushiyama 886, Aoi-ku, Shizuoka 420-8688, Japan.

Corresponding author:

Prof. Nobutaka Hattori, MD, PhD,

Department of Neurology,

Juntendo University School of Medicine, 2-1-1 Hongo, Bunkyo-ku, Tokyo 113-8421, Japan.

Phone: +81-3-3813-3111; Fax: +81-3-5800-0547;

E-mail: nhattori@juntendo.ac.jp

Disclosure: The authors report no disclosures relevant to the manuscript.

Word count for paper: 2422

Word count for abstract: 168

Character count for title: 149

Number of references; 20, tables; 3 and figures: 3, online-only supplements 1.

Keywords

Neurodegeneration with brain iron accumulation, beta-propeller protein-associated neurodegeneration, parkinsonism, intellectual disability, WDR45.

Abbreviations

NBIA; Neurodegeneration with brain iron accumulation, BPAN; beta-propeller protein-associated neurodegeneration.

ABSTRACT

Neurodegeneration with brain iron accumulation (NBIA) is a genetically heterogeneous disorder characterized by the accumulation of iron in regions such as the basal ganglia. We enrolled 28 patients with childhood intellectual disability and young-onset parkinsonism (≤ 40 years at onset) and four patients with infantile neuroaxonal dystrophy. All had been clinically diagnosed and the prevalence of genetic mutations linked to NBIA [*PANK2* (exon 1–7), *PLA2G6* (exon 2–17), *C19orf12* (exon 1–3), *WDR45* (exon 2–11), *COASY* (exon 1–9), *FA2H* (exon 1–7), and RAB39B (exon 1,-2)] were evaluated. We detected seven female patients (25.0%, 7/28) with de novo heterozygote *WDR45* mutations, which are known to be pathogenic for beta-propeller protein-associated neurodegeneration. All seven patients had common clinical features. Pathogenic mutations in other NBIA genes were not found. We also screened 98 patients with early onset parkinsonism without intellectual disability, and 110 normal controls of Japanese origin for *WDR45* mutations. None had *WDR45* mutations. Our data suggest a high frequency of beta-propeller protein-associated neurodegeneration mutations in the Japanese population.

1. Introduction

Neurodegeneration with brain iron accumulation (NBIA) is clinically characterized by brain iron accumulation in the basal ganglia and other brain regions(Gregory, et al., 2009,Schneider, et al., 2013). Iron accumulation and the presence of axonal spheroids in the brain are pathological hallmarks of NBIA. Parkinsonism, dystonia, intellectual disability, and cognitive decline are common symptoms of NBIA. NBIA genetically can be classified into: (i) NBIA1 caused by mutations in the pantothenate kinase-2 gene (*PANK2*), known as Hallervorden-Spatz disease, pantothenate kinase-associated neurodegeneration (PKAN) or aceruloplasminemia, (ii) NBIA2A and 2B involving *PLA2G6*, infantile neuroaxonal dystrophy (INAD) or *PLA2G6* associated neurodegenration; (iii) NBIA3 involving *FTL*, neuroferritinopathy; (iv) NBIA4 involving mitochondrial protein-associated neurodegeneration caused by *C19orf12*; (v) NBIA5 involving mutations in *WDR45*, known as beta-propeller protein-associated neurodegeneration (BPAN) or static encephalopathy of childhood with neurodegeneration in adulthood (SENDA); and (vi) NBIA6 involving *COASY*, COASY protein-associated neurodegeneratoin (Dusi, et al., 2014,Gregory, et al., 2009,Haack, et al., 2012,Saitsu, et al., 2013,Schneider, et al., 2013). Recently, *RAB39B* (a gene encoding a member of the Rab family of proteins), has been reported as a causative gene of X-linked intellectual disability and early-onset Parkinson's disease (Wilson, et al., 2014). Each gene mutation is associated with different clinical phenotypes such as intellectual disability or developmental delay and all lead to advanced parkinsonism and/or involuntary movements. In particular, *PLA2G6* mutations are well known to be a common cause of both adult-onset dystonia-parkinsonism (PARK14) and NBIA(Paisan-Ruiz, et al., 2009).

BPAN is a distinctive neurodegenerative disorder caused by mutations in WD repeat domain 45 (*WDR45*) which is located on chromosome Xp11.23 and encodes WIPI4 protein (Haack, et al., 2012). WD40 repeat proteins act as hubs in cellular networks and are involved in the autophagy-lysosomal pathway (Stirnimann, et al., 2010). The clinical features of BPAN patients present as intellectual disability in childhood, subsequently, parkinsonism, and progressive cognitive decline in their twenties (Hayflick, et al., 2013,Saitsu, et al., 2013). To precisely define the genotype-phenotype correlations of NBIA, we screened for mutations in six genes implicated in NBIA among 32 patients with intellectual disability and parkinsonism. In this report, we compare clinical features of mutation carriers to previously reported cases and discuss possible pathogenic mechanisms of BPAN.

2. Material and methods

2.1. Participants

Twenty-eight patients (male: female = 10: 18) with intellectual disability in childhood and young-onset parkinsonism (≤ 40 years at onset) and four patients with infantile neuroaxonal dystrophy (INAD) (male: female = 3: 1) that had been clinically diagnosed were selected from a DNA bank of Juntendo University, Tokyo, Japan. All 32 patients were screened for genes linked to NBIA. To verify a de novo status of *WDR45* mutations, parents of the carriers of these mutations were investigated as well. We also screened all coding exons (exon 2 to 11) in *WDR45* in 110 normal controls of Japanese origin (male: female = 54: 56, average age; 60.3 ± 16.5 (±SD) years old), and 98 patients with early onset parkinsonism without intellectual disability (age at onset < 30 years; male: female= 49: 49). All clinical details are shown in Table 2. This study was approved by the ethical committee of Juntendo University School of Medicine. All participants were fully informed and signed consent forms were obtained.

2.2. Sequencing analysis

Genomic DNA was isolated using standard protocol. Primer pairs were used to amplify all protein coding exons of *PANK2* (exons 1 to 7), *PLA2G6* (exon 2 to 17), *C19orf12* (exon 1 to 3), *WDR45* (exons 2 to 11), *COASY* (exon 1 to 9), *FA2H* (exon 1 to 7), and *RAB39B* (exon 1 to 2), and sequenced them by the Sanger method using BigDye Terminators v1.1 Cycle Sequencing Kit and 3130 Genetic Analyzer (Life Technologies, Foster City, CA, USA). PCR and sequence primers were designed using Exonprimer (http://ihg.gsf.de/ihg/ExonPrimer.html). Sequences and PCR conditions are described in supplementary data (Supplementary material and methods and Table 1). Healthy controls were screened for mutations in exon 5-10 because this region contains the mutations identified in patients.

2.3. Reverse transcriptase-PCR analysis

Total RNA was isolated from peripheral blood of four patients using a PAXgene Blood RNA Kit (Qiagen, Valencia, CA, USA). Total RNA was used to synthesize cDNA. Random 9-mer primers (Takara Bio, Shiga, Japan) and M-MLV Reverse Transcriptase (Promega, Madison, WI, USA) were used for the reverse transcription reaction. The

cDNA was amplified by PCR using AmpliTaq Gold 360 Master Mix (Life Technologies, Foster City, CA, USA), and the following primers: 5′-GCGCCATGACAAGATCGTGATC-3′ (forward) and 5′-CAAGGCTCAGCTCTGCAGTTC-3′ (reverse), in between the boundary of exons 5-6 and exon 12 for Case 1, Case 2 and Case 6; 5′-AGAAGGGGCATCTGGACCAC-3′ (forward) and 5′-GTTAATGCAGTAGAGGGTGGC-3′ (reverse), in between the boundaries of exon 3-4 and 8-9 for patient Case 7. Reverse-transcriptase PCR (RT-PCR) products were visualized by 2% agarose gel electrophoresis and each product was sequenced by Sanger method using BigDye Terminators v1.1 Cycle Sequencing Kit and 3130 Genetic Analyzer (Life Technologies).

3. Results

Out of a total of 28 young onset parkinsonism with intellectual disability, 4 INAD, and 110 healthy controls, we found *WDR45* mutations in seven patients among adults (25.0%, 7/28). There were no mutations or variants in exons 5–10 in controls. In contrast, pathogenic mutations in *PANK2*, *PLA2G6*, *C19orf12*, *COASY, FA2H* or *RAB39B* were not identified. We detected one mutation p.R635X in *PLA2G6*, this mutation was identified in heterozygote form and was therefore not considered pathogenic. In addition, screening for *WDR45* mutations in patients with early onset parkinsonism without intellectual disability failed to identify any mutations. Therefore the frequency of *WDR45* mutations is prominently high and specific for NBIA patients (table 1). All mutation carriers were female without any family history. Clinical overviews of these cases are summarized in Table 2 and the history of present illness is described in the Supplementary data; the details of clinical course of each patients. In total, we detected six different mutations in *WDR45* comprising two frame-shift mutations, one nonsense mutation, one inframe deletion, and two missense mutations (Figure 1). All mutations were located in exons 5-10. Two mutations at c.400C>T (p.R134X) and c.293T>C (p.L98P) have been previously reported (Haack, et al., 2012,Hayflick, et al., 2013) whereas the other four are novel. The c.628T>C (p.S210P) in exon 8 is a novel missense mutation, and the position of the amino acid is highly conserved in many species (Supplementary Figure 1). None of the patients presented a positive family history of disease; thus to assess whether the identified mutations are de novo, we screened the all the available parents of mutation carriers. DNA was available for both parents for Case 1, 2, and 6; and the mother of Case 3 and 7; unfortunately DNA was not available for parents of Case 4 and 5. This analysis failed to identify any of the *WDR45* mutation in patients' parents. cDNA sequencing indicates a selective expression

of the mutant allele for Case 1 and 7, and expression of both alleles for the mutation identified in Case 2 and 6. Indicating that WDR45 gene has two types of transcription (Figure 2).

Clinical course showed that patients with WDR45 mutations had two phases in the progression of the disease: (1) intellectual disability and febrile seizures in childhood, and subsequently (2) parkinsonism and advanced cognitive decline in adulthood after their twenties (Table 2). In six cases (except for case 3) there was noticeable progressive cognitive decline coinciding with the onset of parkinsonism. All cases had intellectual disability in childhood, commonly accompanied with high prevalence of febrile convulsion at infant stage (85.7%, 6/7). Five patients did not have verbal communication, two patients had limited vocabulary. In adulthood, Mini-Mental State Examination (MMSE) could not be evaluated due to severe cognitive problems and language impairment. In terms of parkinsonism, akinesia, rigidity and postural abnormality were prominent from 32.0 ± 3.70 years old, but tremor and dystonia were lesser symptoms. Increased deep tendon reflexes were seen in half of patients (57.1%, 4/7), and pathological reflexes such as Babinski's sign appeared at a higher prevalence (85.7%, 6/7). None of the patients had complications of psychiatric symptoms. A good response to levodopa was seen in all patients (100%, 7/7). Three patients in particular (Cases 4, 6, and 7) showed excellent response to medication; Case 4 showed marked improvement of gait after taking levodopa (300 mg), cabergoline (3 mg), and pramipexole (1.5 mg/day); in Case 6 rigidity in all limbs was improved by levodopa (300mg), ropinirole (0.75mg), and trihexyphenidyl (4mg/day), and in Case 7 gait ability and akinesia was improved by levodopa (200mg/day). Four patients developed levodopa induced dyskinesia (57.1%, 4/7). Four patients had history of epileptic discharges (57.1%, 4/7). Electroencephalogram abnormalities were detected among three patients (60%, 3/5). Rett-like hand stereotypies, sleep problems, and ocular defects were not prominent. Brain magnetic resonance imaging (MRI) imaging indicated characteristic features such as high intensity in T1 weighted images (T1WI); halo, and low intensity changes in T2 weighted images (T2WI) in the substantia nigra, the globus pallidus and cerebral peduncles in all examined cases. Cases 2, 3, 4, 5, and 6 showed diffuse atrophy of the cerebrum (Figure 3). Case 3, 4, and 6 demonstrated disproportionately hemisphere atrophy. Only Case 6 had cerebellar atrophy. Brain MRI assessment of all six cases showed no evidence of eye-of-the-tiger sign and white matter involvement. The single photon computed tomography (SPECT) of three cases (3, 6, and 7) indicated non-specific hypoperfusion; bilateral frontal and left temporal lobe regions in Case 3, right frontal, temporal, occipital, and parietal lobe in Case 6, and bilateral occipital lobe in Case 7.

4. Discussion

We found seven patients with heterozygous *WDR45* mutations, five of whom had not been previously described. In our cohort, the prevalence of the *WDR45* mutations was higher among NBIA patients (18.4%) compared with other genes implicated in NBIA and were only found in the specific cohort of intellectual disability and young-onset parkinsonism. To our knowledge, there are no reports of a comprehensive cross-sectional study of a single cohort presenting the same symptoms for mutations in NBIA genes. The precise prevalence of mutations in each gene still remains unknown. However, previous data indicates the prevalence of mutations in NBIA is 35–50% for *PANK2*, 20% for *PLA2G6*, and 6–10% for *C19orf12* (Hartig, et al., 2011,Hayflick, et al., 2013,Hogarth, et al., 2013). The distribution observed in our population is quite distinct and this is likely owing to either our focus on patients with intellectual disability in childhood and young-onset parkinsonism (≤ 40 years) or ethnically specific differences between studied populations. In addition, our sample size is small (n=32), and further studies are needed to accurately evaluate the prevalence of mutations in these genes.

All patients with *WDR45* mutations had two phases of disease course, similar to that reported previously (Haack, et al., 2012,Hayflick, et al., 2013,Ichinose, et al., 2014,Rathore, et al., 2014,Saitsu, et al., 2013,Verhoeven, et al., 2014). We reviewed all available clinical data of patients with BPAN from previous reports and our current study (table 3). Interestingly, all 40 patients with BPAN present common clinical features such as high prevalence of intellectual disability (100%; 40/40), progressive cognitive dysfunction in adulthood (100%; 40/40), dystonia (90.0%; 36/40), good response to levodopa (86.0%; 19/22), parkinsonism (90.0%; 36/40), and T1WI; halo, and low intensity changes in T2WI in the substantia nigra, the globus pallidus, and cerebral peduncles of brain MRI (100%; 37/37). Interestingly, the majority of the *WDR45* mutation carriers described in our study and others(Haack, et al., 2012) are female (female: male = 49:4), but the clinical features observed in males appear to be similar to those of females(Hayflick, et al., 2013).

Since the clinical features of BPAN are specific and distinct from other types of NBIA such as PKAN, INAD, neuroferritinopathy, mitochondrial protein-associated neurodegeneration and COASY protein-associated neurodegeneratoin; it may be used to specifically establish a diagnosis. For example, BPAN does not involve optic